Proceedings of the 10th Brazilian Congress of Thermal Sciences and Engineering -- ENCIT 2004
Braz. Soc. of Mechanical Sciences and Engineering -- ABCM, Rio de Janeiro, Brazil, Nov. 29 -- Dec. 03, 2004

Paper CIT04-0688

QUANTITATIVE VISUALIZATION OF EARLY FROST GROWTH WITH SCANNING CONFOCAL MICROSCOPY

John G. Georgiadis
Mechanical & Industrial Engineering Dept. and Bioengineering Dept.
University of Illinois at Urbana-Champaign, IL 61801, USA
georgia@uiuc.edu

John Hoke
Innovative Scientific Solutions Inc., Dayton, OH 45440, USA
john.hoke@wpafb.af.mil

Abstract. *Frost in most terrestrial applications (refrigeration, cable or wing icing) consists of frozen dew that is deposited on a cold surface exposed to humid air. In an attempt to understand the early growth phase of frost (from inception to a few hundred micrometers in thickness), a systematic study aiming at collecting morphological information at the near-micron range is reported here. We present here a high-resolution, video rate (up to 30 frames per second) visualization of frost forming on horizontal substrates under forced convection conditions. Near-micron resolution of the crystalline microstructure is achieved by employing source-scanning confocal microscopy in reflection mode with axial translation (parallel to the objective lens axis) of the sample. This technique obviates the difficulties with conventional microscopy by increasing contrast and allows 3-D and time-resolved quantitative visualization of the frost morphology. The successful design of a miniature wind tunnel that allows local heat transfer measurements in addition to optical access is also described here. Our results reveal two basic frost inception scenarios: (A) dropwise condensation and freezing or (B) direct ice deposition from the vapor phase (ablimation). Furthermore, the reconstruction of early frost morphology during scenario A provides unique insights into the effect of substrate wetting properties on frost morphology, the most important of which is that frost grown on hydrophilic substrates tends initially to be thinner and denser than that grown on hydrophobic substrates.*

Keywords. *Frost, dropwise condensation, confocal microscopy.*

1. Introduction

When vapor-laden air is brought into contact with a cooled surface at a temperature below the dew and freezing points, water driven by vapor pressure gradients is deposited on the surface and frost ultimately develops. A thorough understanding of the fundamentals of frost formation is crucial to the refrigeration industry. In air-to-air heat pumps and refrigeration equipment, most studies have focused mainly on the economics of alternative defrost schedules. It has also been estimated that performance and reliability considerations cause designers to oversize refrigeration equipment by 50% to ensure capacity under frosting conditions, and that frost is responsible for a 25% degradation in average system performance. The literature on the effects of frost on flexible structures exposed to the weather is dominated by the problem of cable instabilities caused by the combination of wind with rain or rime ice, cf. Verwiebe and Ruscheweyh (1998). Seeking to explain incidents involving the catastrophic collapse of power lines, suspension bridges and the like, the available research focuses primarily on the vibration of the frosted components and secondarily on the deposition of water on ice. In contrast, there is an increasing awareness on the effect of early frost roughness on the aerodynamics of lifting surfaces as it pertains to the problem of anti-icing of planes, cf. Henry *et al.* (1995).

Frost growth can be divided into two stages: an early, relatively short crystal growth period, and a mature frost layer growth period. Designing frost-free surfaces requires the complete structural characterization of frost during the early period. Defrosting or suppressing the growth of frost requires similar information during the later period. In both cases, fast high-resolution techniques for in-situ characterization of the frost layer are needed. Frost consists of a lattice of fragile ice crystals in the form of a light-scattering heterogeneous porous medium. It is therefore very difficult to estimate its density (or porosity) distribution or to measure interstitial temperature distributions directly.

There is a plethora of *macroscopic* empirical and analytical studies of mature frost growth, see for example O'Neal and Tree (1985) and references therein, as well as Kondepudi and O'Neal (1989, 1990) and Tao *et al.* (1993). Mature frost growth rates are consistently found to increase with humidity and surface-to-air temperature difference. Using numerical simulation, Tao *et al.* (1993) showed how the complex behavior of the local heat and mass transfer coefficients affects mature frost growth on a clean cold surface. Good agreement with experimental data was reported, provided that the *proper* transport properties are used. The relationship between frost thermal conductivity and density is strongly affected by the details of the microstructure of frost. An exceptionally detailed study of early frost growth, replete with measurements of thickness (up to 1.5 mm), density, as well as the effect of substrate contact angle to water, was published by Seki *et al.* (1984). They found that the frost thickness observed on the hydrophilic substrate is higher than the hydrophobic one, while the opposite trend was observed for frost density. The average density was found to

decrease to a minimum value after 25 to 50 minutes from inception and then to steadily increase. It should be noted that the observations reported in Seki *et al.* (1984) correspond to frost thickness from approximately 0.1 mm to 1.5 mm, as measured with a micrometer and a spring-loaded cross slide, and density measurements that were made by scraping frost off the substrate and weighing it. Semi-empirical relationships using the density (or porosity) as a parameter are not satisfactory for the early frost growth period, cf. Sahin (2000) and references therein. Using an innovative optical method to measure average frost thickness, Storey & Jacobi (1999) proposed a scaling relationship between mature frost thickness growth and time, which succeeds in reducing the scatter of experimental data in fairly complex grazing flow fields within one adjustable parameter associated with a putative conductivity-density linear relationship. Again, deviations were observed during the early frost growth period. In one of the rare studies to carefully consider the effect of substrate surface energy, Dyer *et al.* (2000) found significantly higher mature frost growth rates (frost thickness vs. time) on the hydrophilic substrate (which is in agreement with the results of Seki *et al.* (1984)) and attributed them to differences in layer thermal resistance, which in turn relates to the initial coverage at the early growth stage. We feel that every attempt to derive thermophysical properties of frost, should start from the microstructure and account for the substrate surface physics.

Microscopic experimental studies of frost deposition on *well-characterized substrates* have only recently started to appear in the heat transfer literature. Hoke *et al.* (2004) made careful microscopic observations of frost deposition on clean glass (hydrophilic) and polytetrafluoroethylene (hydrophobic) substrates and found that, in contrast to early growth behavior, the thickness of the frost layer during the mature growth increases faster on substrates that have lower contact angles, and the frost density is less than that measured for high-contact angle substrates. This behavior was explained in terms of the effects of substrate wettability and its impact on condensate distribution growth: a higher conductivity layer is formed on the hydrophilic than on the hydrophobic substrate. A model was employed to account for the experimental data and bolster the hypothesis that substrate wettability affects mature frost growth through its effect on condensate distribution at frosting inception. Hoke, Ramaswamy and Georgiadis (2004) have recently reported a systematic microscopic investigation of the transition from condensation (supercooled liquid layer) to ablimation (direct vapor to ice deposition) over a clean glass substrate exposed to a constant grazing air flow kept at atmospheric pressure and –16°C, and in the range of 47%-93% relative humidity ratio. By repeating the observations of the growth pattern with SCM for various humidity ratios, they reported the demarcation of boundaries in the temperature-vapor saturation ratio space which delineate the parameter domain where condensation or ablimation are preferred. The transition from condensation to ablimation is found to occur between –33 and –35°C and a vapor pressure of 0.13-0.15 g/kg.

The present study is motivated by the scarcity of quantitative data obtained in-situ during the period immediately preceding and following frost inception. We report here the novel use of Scanning Confocal Microscopy (SCM) for high-resolution (near-micron) visualization of frost during the early growth phase, effectively corresponding to frost layers less than 500 μm in thickness. The scope of the present manuscript is confined to the frost scenarion involving condensation to freezing which occurs at higher temperatures. This study is in essence the culmination of studies by Greywall (1994), Georgiadis (1994, 1997), Georgiadis *et al.* (1994), Georgiadis and Ramaswamy (1995), and Ramaswamy *et al.* (1995). We describe (1) the design of an apparatus that accepts interchangeable substrates and is inserted under the objective lens of the SCM, (2) the establishment of systematic experimental protocols and standardization of substrates, and (3) the in-situ visualization and measurement of crystal-level morphological parameters of early frost. The presentation starts from the description of the imaging setup and proceeds with qualitative and then quantitative observations of frost formation.

2. Experimental Methodology

2.1. Scanning Confocal Microscopy (SCM)

The conventional (wide-field) light microscope receives light from planes above and below the plane of focus. This results in a long depth of field and loss of depth discrimination. In contrast, the working principle of confocal microscopy is that only one plane perpendicular to the line of view is in focus at a time. Effectively, by using a very narrow depth of field and by limiting the field of view, the instrument can produce very sharp images. Confocal microscopes have a strong *optical sectioning* property: one can reconstruct a three-dimensional surface by moving the in-focus plane (z-sectioning) and recording the intensity of the collected light. Our SCM system generates a scanning laser beam (point illumination source) to illuminate the object and detects the reflected light with a point detector. The image is formed by digitally summing the signal as the z-stage (driven by a stepper motor) moves the object (which is fastened on the z-stage) through the focal plane of the objective lens. Since the signal intensity peaks when the focal plane crosses areas of strong index of refraction gradients (such as the ice-air interface), the SCM can perform non-contact profilometry of complex surfaces.

Figure 1 depicts our experimental setup along with image processing and analysis hardware. The SCM system is built around a conventional Nikon microscope operating in reflection mode. The system consists of a confocal optical

system, a linearly polarized laser illuminating source (1.5 mW He-Ne 632.8 nm), a video-rate beam scanner, a linear CCD sensor, a z-axis controller, a signal processing unit, and a video monitor. Through the use of a scanning mirror for y-, and an acousto-optical deflector for x-scanning, a polarized beam is raster-scanned at video rates over the field of view. It takes as little as 1/30th of a second to obtain the image of the in-focus slice, with a number of slower scanning rates available. SCM improves spatial resolution and depth discrimination by rejecting out-of-focus light with a detector pinhole with a narrow slit aperture. The resolution is improved by a factor of two at the expense of the field of view, but the latter is recovered by scanning the confocal spot on the object in a raster pattern on the xy-plane normal to the z-axis. The design of the optical system also allows the re-orientation of the beam path and the operation under conventional reflection microscopy with a simple turn of the eyepieces. A SONY BXC 107A CCD camera attached to the eyepiece through an adapter tube provides the extra capability of recording under bright-field illumination conditions.

In order to achieve long working distances that are crucial in non-contact frost profilometry, we used a set of NIKON CF M Plan Apochromat objective lenses (10X, 20X, 40X, 100X) of low numerical apertures (0.25, 0.35, 0.40, 0.75, respectively) and 210 mm tube length. The 100X objective gives the highest magnification of 4800X (on a 14" monitor) but with a short working distance (4.7 mm) and a narrow field of view (45 μm). Recall that low numerical aperture implies lower resolution in the z-axis and lower image intensities, but it also reduces shadowing artifacts during the imaging growing frost (since the beam aperture is narrower).

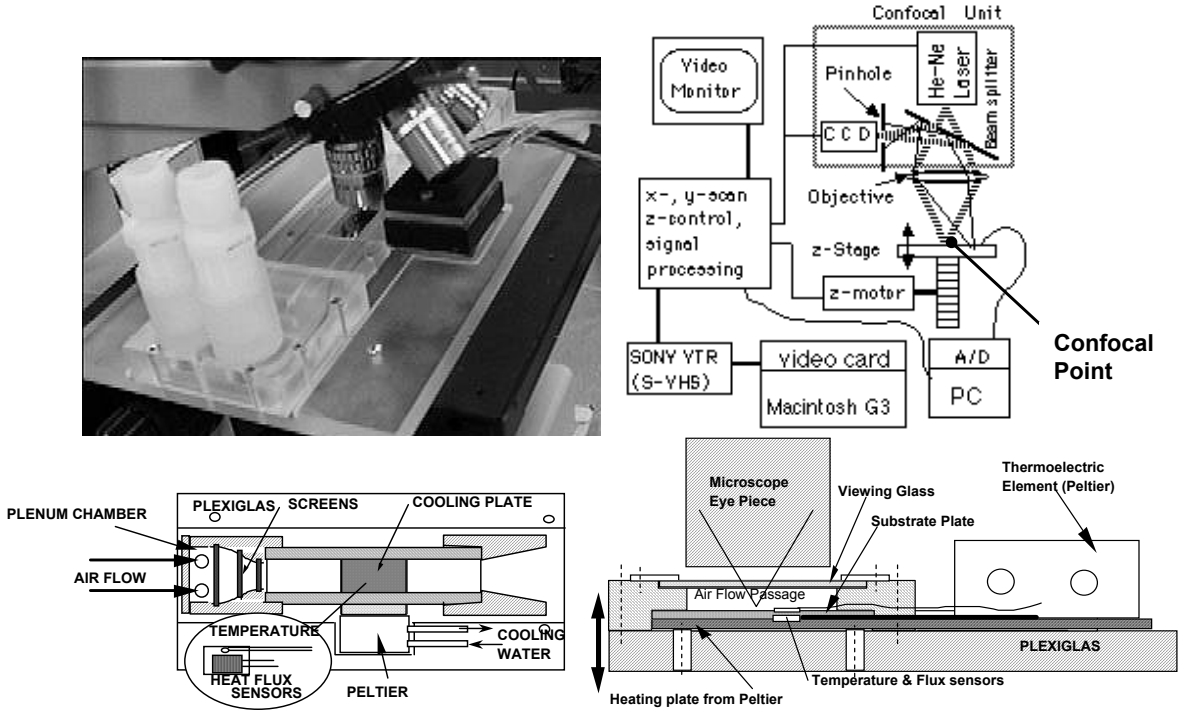

Figure 1. Scanning Confocal Microscopy (SCM) for high-resolution visualization of frost during the early growth phase and the miniature wind tunnel and is inserted under the objective lens of the SCM and allows the exposure of interchangeable substrates to forced convection humid air flow.

2.2. Experimental Setup

We fabricated and instrumented a 125 mm long wind tunnel of rectangular cross-section (3 mm height and 17.6 mm width) by joining two machined plates of Plexiglas. The distance between the viewing glass top and substrate plates is constrained by the lens with the smallest working distance corresponding to the the 100X objective lens. The substrate plates were heated/cooled by a thermoelectric element which is capable of imposing a temperature in the range -20^{o}C to +100^{o}C at the root of the substrate plate (with 0.1^{o}C accuracy) and deliver up to 12 Watts of cooling power. The substrates plates were pressed towards the upper half of the wind tunnel with set screws (refer to Figure 1). Good thermal contact between the substrate plates and the cooling plate connected to the thermoelectric element was ensured by using a high thermal conductivity thermal paste (Omegatherm 201). A heat flux sensor (Omega HFS-4, 10% accuracy) is sandwiched between the plates to record the heat flux and temperature between the substrate and the Peltier plate. This heat flux sensor is about 0.254 mm thick and also has a K-type thermocouple encapsulated with it. An E-

type thermocouple was employed over the substrate plate to record the surface temperature. All thermocouples were calibrated to yield an accuracy of about 0.3^{o}C.

Dry air was supplied from a compressed-air tank at room temperature through a 19 mm hose and was branched off downstream of a fine metering control valve. The control valve is used to regulate the airflow rate through the wind tunnel. One air stream becomes fully saturated after bubbling through water and is then mixed with the other dry air stream. After mixing, the humidified air passes through a 25.4 mm box in which the humidity sensor is housed. This thin film sensor (Vaisala model HMP 233) gives both the relative humidity and the dry bulb temperature of the air stream with an accuracy of ±2% and a response time of 15 seconds (90% rise) for the relative humidity, and an accuracy of ±0.1^{o}C for the temperature. The humidified air is routed through a low-flow rate flowmeter. The flow meter gives a 0-5 Volts output that is recorded with the data acquisition system.

Thermocouple data were acquired using LABVIEW^{TM} and a National Instruments NB-MIO-16H-9, 12-bit A/D board connected to a SCXI 1100 32-channel multiplexer by the same manufacturer. In addition, the heat flux through the substrate was monitored by an accurate digital multimeter, after the output of the thin film sensor was converted on the basis of a calibration curve provided by the manufacturer. All measurements were recorded with a personal computer using customized software that reads data from the digital multimeter through the computer's serial port and reads data directly from the A/D board plugged in the computer. A time stamp is tagged to the data using a 100 μsec clock on the A/D board. The data reported here is acquired at 0.3 Hz. The thermocouple temperature values are averaged 30 times each over a period of 3.34 seconds, and the heat flux measurement using the digital multimeter are made at a setting accurate to within 0.1 μV with 100 PLC analog averaging. The heat flux sensor has a response time of 0.72 seconds for a 62% rise.

2.3. Experimental Procedure

Three types of substrates were used in this phase of the investigation: glass slides, thin plates cut from heat-exchanger aluminum fin stock (formed by extrusion), and thin aluminum films vapor-deposited on silicon wafers. The fin stock was 0.1 thick and had scratches and scars from regular handling, in addition to the grooves formed during the extrusion process. The thickness of the aluminum film was about 0.25 μm and the available area is about 6mm X 6mm. Using a profilometer, the surface was scanned and the centerline average roughness was found to be about 16 nm. The average roughness is defined according to American National Standard Institute (ANSI) B46.1-1978.

The samples (in the form of solid plates cooled from below) are positioned under the microscope objective and the thermodynamic state of air stream is established by controlling the humid/dry air bypass and the heat exchangers for the wind tunnel and substrate. The video encoder of the SCM signal processing unit generates analog video that is recorded to the frame-accurate VCR (activated by the operator when condensate or frost appears), while the z-stage (on which the tunnel is mounted) is controlled by the personal computer or manually. The same personal computer acquires data and sends the outputs required for the various controls. Fast video rate scanning (30 frames per second, or in smaller frequencies) allows the visualization of moving interfaces. Synchronization of the video record with the sensor (digital) data stream is achieved via an improvised video “clap board” that is driven by LABVIEW software and the 1 MHz clock of the A/D board. The data acquisition computer interfaces serially with the signal processing unit of the SCM and enters alphanumeric strings on the appropriate video frame: the word “start” is stamped on the frame of video indicating the start of the digital data acquisition stream. In conjunction with the timing device of the VCR, this procedure allows video-time series synchronization within 2 frames (approximately 1/15 sec). Image and data processing is performed off-line.

The video can be reviewed frame by frame and the frame marked with “start” can be located during post-processing. The video recorder outputs analog (S-VHS) video at a "slow" rate to a graphics workstation or other personal computers via appropriate frame capturing boards. After the useful segments of the original video stream have been sampled and digitized, 3-D image reconstruction can be performed off-line using available image analysis software. Basically, the data are organized into 3-D "snapshots" of the interface, with each snapshot corresponding to a stack of z-slices obtained at known z-elevations. Measurements and calculations are made using available image analysis software. The surface profile corresponds to the areas of maximum intensity in each slice. Finally, a sequence of meaningful frames or 3-D "snapshots" can be animated and recorded back to the video deck for purposes of demonstration.

3. Qualitative Visualization

Following numerous observations of frost on a substrate that is exposed to humid grazing flow at approximately 1 atm pressure, we have identified two paths towards frost formation during its early phase (crystal growth):

A: Vapor → Liquid (condensation) → Ice (freezing) → Ice (ablimation)

B: Vapor → Ice (ablimation)

Path A is typical in air streams above -35^{o}C and is realized as soon as the substrate surface reaches the corresponding dew point. Water deposits on the cold substrate in the form of dropwise condensation, or thin liquid films if the substrate is hydrophilic. The droplets coalesce to form larger droplets, which eventually freeze when a high degree of supercooling is reached (approximately -10^{o}C). From then on, ice growth proceeds directly from the vapor phase (ablimation). Ice crystals appear on the surface and around frozen droplets, gradually filling the space between the drops and forming closed rings. The size of the droplets (before their growth is arrested by the frost rings mentioned above) decreases as we decrease the surface temperature since ice nucleation occurs earlier.

Figure 2 exemplifies the behavior of condensate just before frost inception during path A. As the freezing front advances inwards from the periphery of the droplet-substrate interface, the droplet dilates (as ice expands). A frequent phenomenon during incipient freezing is the disappearance of near-micron size "satellite" droplets (marked by the letter F in the frames) in the vicinity of freezing droplets. This can be attributed to the water vapor pressure difference created during freezing: ice has lower vapor pressure than liquid water at the same temperature. According to our observations, such small droplets do not freeze but evaporate to the large freezing droplet in their vicinity. Tentacle-like bridges emanate from each freezing droplet and induce the nucleation of adjacent supercooled droplets upon contact.

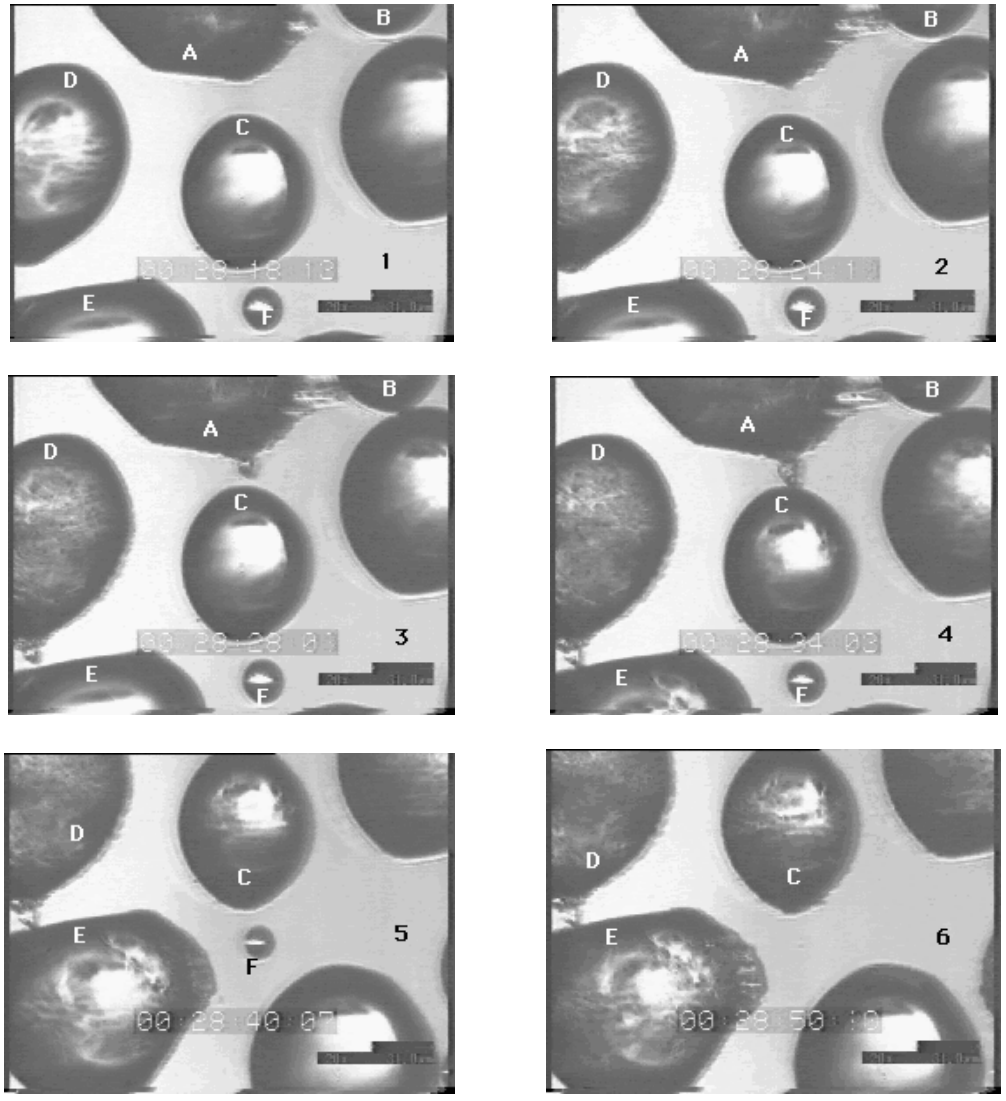

Figure 2. Frame sequence (roughly 6 sec apart) showing the interaction and freezing of supercooled droplets near the frost inception. F marks the satellite droplet which evaporates. The long dark bar at the lower right of each image corresponds to 60 microns.

Path B appears in extreme conditions (very cold and dry air streams) and is marked by a direct ablimation step and subsequent ice crystal growth. This path has been systematically described by Hoke, Ramaswamy and Georgiadis (2004). As with all nucleation phenomena, the role of the substrate surface (which acts as a catalyst) is of paramount importance during the early phase of frost growth. It is rather straightforward to demonstrate that by mechanically removing (wiping) the frost after the completion of path A, new frosting occurs via path B. Technically, this does not fall under the scenario for path B since freezing is catalyzed by the microscopic ice crystals smeared on the surface following the shearing of frost from the previous icing cycle. We have also managed to eliminate path A in favor of B for the same thermodynamic conditions by manipulating the surface finish.

4. Quantitative Visualization

In Figure 3 we present a reconstructed image of the frost layer formed on the fin stock plate cooled at -3^{o}C from below and exposed suddenly to 22^{o}C stagnant ambient air from above. We are viewing the 3-D rendered object at an angle. This is a portion of the original 3-D structure that was acquired with 700 μm field of view. Fourteen z-sections (10 μm apart) were acquired and digitized to create the composite. A columnar crystal is shown on the upper left corner of the image. Although contrast is improved in SCM, optical sectioning artifacts persist but they depend upon the specific sample. In order to assess the accuracy of the z-sectioning of our SCM system, we imaged 10 micron glass beads suspended in water. On the basis of the distortion of the bead images, we estimate that the overall uncertainty in the z-direction is 5 μm for the 40X lens. This loss of depth resolution is a consequence of complex spherical aberration and scattering of the beam as it traverses translucent objects. Because of the difference in refractive index between the glass bead (n=1.5) and water (n=1.3), the bead surface is no longer in focus. The focal plane is distorted and moves upwards since the glass bead has higher index of refraction than the surrounding medium (water). Although this is a simplified model of the refraction of the laser beam impinging on the ice crystals during the imaging of frost layers, the same problem occurs during the condensation of water drops on hydrophilic substrates.

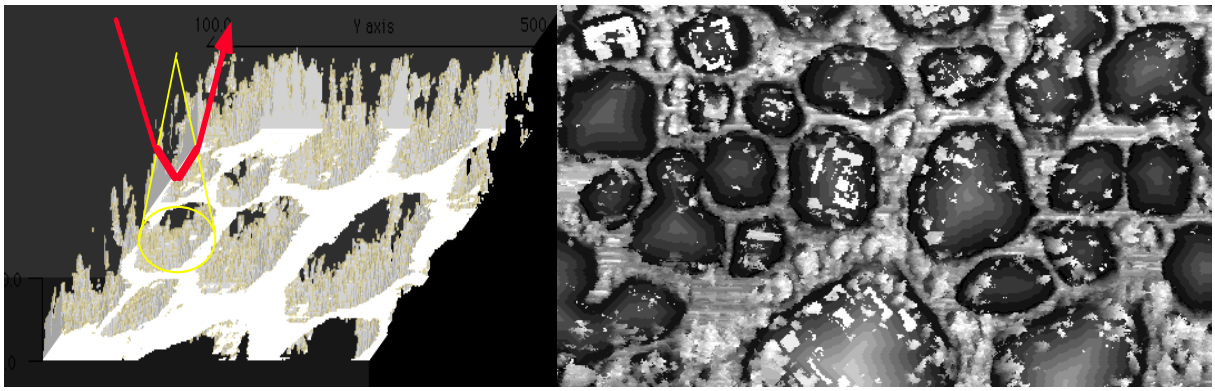

(a) (b)

Figure 3. (a) Three-dimensional reconstruction of early frost with scanning confocal microscopy (view from below). (b) View (from above) of reconstructed frost surface perpendicular to the substrate surface. The horizontal side is 700 microns long.

We have performed a systematic investigation of frosting over three types of substrates (glass, fin stock, thin aluminum film on silicon) in order to examine the effect of surface physics on frost density. The experiments were conducted with T_{sub}= -3^{o}C to -5^{o}C, and T=20 ^{o}C to22 ^{o}C with 20-30% relative humidity, and U=0.5 m/sec. These conditions correspond to frost inception according to path A. Experiments were conducted for the 0.1 mm-thick substrate made from aluminum fin stock with focus on the transient heat transfer phenomena near frost inception during a typical “cool-down” period and re-freezing after defrost. The free-stream air conditions were set to 23.5^{o}C (dry bulb temperature) and 14% relative humidity that correspond to a dew point of -4^{o}C. The mean velocity of the air was set at U=0.6 m/sec and U=1 m/sec, which are equivalent to Reynolds numbers of 114 and 191 (based on the channel's height), respectively. The root of the Peltier plate was set to T= -15^{o}C and T= -18^{o}C. Figure 4 (a) gives the corresponding heat flux measurements, with the negative sign denoting flux from the air stream towards the substrate. All experiments have been repeated at least twice: the solid and dash line pairs represent runs over an originally dry substrate (solid line) and then their repetition (dash line). There are two prominent features for the T=-15^{o}C case: a "kink" at about t=100 sec and a "spike" in the vicinity of t=200 sec. The "kink" corresponds to the leveling of the substrate temperatures and the

growth of the condensate film on the surface (which increases the thermal resistance at the solid-air interface). This feature is missing in the T=-18^{o}C case and this can be attributed to the fact that the substrate temperature falls continuously for that case. The second feature (sharp spike) corresponds to the freezing of the (supercooled) droplets and its magnitude denotes the amount of heat released from the ice towards the substrate. An estimate of this energy is obtained for the T=-18^{o}C; U=1 m/sec case, by measuring the area inside the spike in Figure 4(a). The estimate is 1,722 Joules/m^2 that is almost half of a measurement of 3,660 Joules/m^2, the latter obtained by estimating the latent heat corresponding to the volume of ice in the field of view at frost inception. The difference can be attributed to at least three factors: (1) the heat flux sensor gives a surface-average measurement over an area much larger than the field of view, (2) there is a possibility of extra ice formed in the deep surface grooves, and (3) the heat flux sensor signal has a finite rise time and, therefore, sharp rises are under-predicted. Similar spikes in heat flux have not been observed during path B (ablimation) since the latent heat is released continuously through the phase of water deposition. Finally, we observe a consistency in the time and location of frost inception during the repetition of the experiment, a fact that has corroborated by numerous experiments.

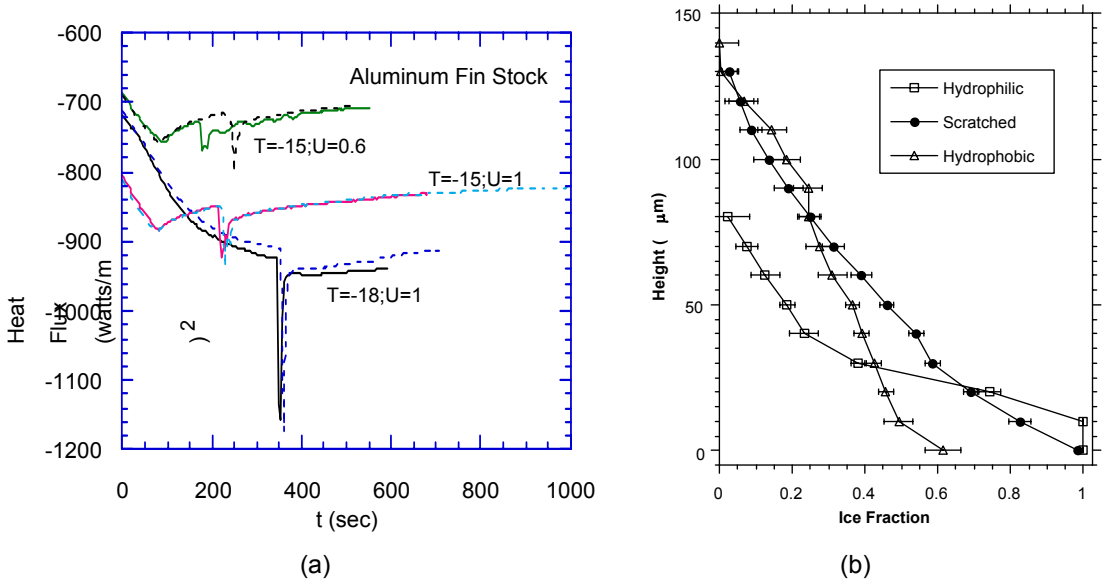

Figure 4. (a) Heat flux through aluminum fin stock substrate for different cooling plate root temperatures (T) and mean air velocities (U). Shown are results for two runs per T, U combination: an experiment over an originally dry substrate (solid curve) and then its repetition (dashed curve). (b) Measurement of the average frost (ice) solid fraction as a function of z-position (height from cold substrate) for three different substrates. SCM gives optical slices with intensity maxima corresponding to the intersection of theses slices and the free surface. The ice fraction at each height is estimated by computing the average grayscale value over the corresponding slice.

We have used commercially available software packages to estimate the density of frost from the raw data of SCM obtained with all three substrates. These estimates are obtained by averaging frost sections over constant z-planes. Figure 4(b) gives the variation of the frost density (expressed in terms of the volumetric fraction of ice) as a function of height above the substrate and at 5 min after the inception of frost. The error bars correspond to the variation of the measurements among 3 repetitions of frost growth on each substrate. The substrates are characterized as "hydrophilic" (clean glass –microscope slides), "scratched" (aluminum fin stock), and "hydrophobic" (aluminum film) on the basis of the apparent wetting angle of water deposited on them. A liquid layer of ~20 µm thickness covers the hydrophilic substrate, on which frost crystals appear. The frost grown on the hydrophilic substrate is the most dense of the three cases. It is interesting to note that the frost layer on the scratched aluminum is as tall as that corresponding to frost growing on the hydrophobic substrate, although the latter has only 60% surface ice coverage vs. 100% of the former. These results demonstrate the profound effect of substrate chemistry and might explain the scatter in mature frost density measurements reported in the literature. The thickness of frost grown on the hydrophilic substrate is lower than that for the hydrophobic. Although in apparent contradiction with the findings of Seki *et al.* (1984) and Storey & Jacobi (1999), the reader is reminded that the observations reported here are for the *early* frost growth phase. Our observation that the frost grows *initially* thicker on hydrophobic substrates is verified by underway systematic observations of frost inception on functionalized substrates (i.e. plates coated with well-characterized thin films) and is consistent with the

shape of the supercooled droplets immediately following freezing (depicted in Figure 2). The growth rate of frost depends on the effective thermal conductivity of frost layer that is changing during its densification (consistent with Seki *et al.* (1984)). Our working model of further growth calls for lower thermal resistance for hydrophilic substrates (owing to elevated surface coverage), with subsequent faster growth of secondary ice crystals that results in longer dendrites and overall thicker mature frost. The last assumption is also consistent with the observation of Seki *et al.* (1984) of lower overall frost density for frost grown on the hydrophilic substrate.

5. Conclusions

In order to understand frost and assess the efficiency of any anti-frost methodology, one needs first to probe the early stages of frost growth. When a humid air stream is brought into contact with a cooled surface at a temperature below the dew and freezing points, two frosting scenarios are observed: (A) condensation followed by subsequent freezing, or (B) direct ablimation (vapor to ice transition). Frost being a fragile and ephemeral porous medium, only full-field non-invasive techniques are candidates for an in-situ investigation. We have been able to visualize quantitatively the frost evolution in-situ with unprecedented resolution using Scanning Confocal Microscopy (SCM). The samples (flat surfaces) are placed in miniature wind tunnels under thermal control and moved along the axis (z) of the SCM objective. A large number of images are acquired during repeated z-sectioning by moving the z-stage incrementally. In addition to the observation of droplet-frost interaction, SCM provides high-resolution three-dimensional visualization of frost structure very near the cold surface, which allows the measurement of frost density and the local heat transfer rates.

We have focused here on the fundamentals of early growth of frost formed in typical engineered systems and our results have established the following facts:

1. Most visibly upon frost inception on hydrophobic substrates, satellite droplets “evaporate” near the freezing front. Although this scenario is already ensconced in the literature, it has not been directly demonstrated until now. Nevertheless, this phenomenon can account for macroscopic observations of frost maldistribution in industrial condensers with numerous fin arrays.
2. During path A, hydrophobic substrates accrue taller/leaner ice with less surface coverage than hydrophilic substrates, for the same thermodynamic conditions. There is ample indication that the trends in frost height reverse later [14,21], on account of the postulated better heat conduction through the denser early frost deposited on hydrophilic substrates.
3. Frost inception according to path A is characterized by a quick release of latent heat manifested by a sharp spike in the heat flux towards the substrate, in contrast to path B. The location and time of frost inception are consistent between repetitions of the frosting experiments on the same substrate.

We believe that SCM should be added to the arsenal of quantitative visualization methods, cf. Georgiadis [22], because of its great potential in visualizing the evolution of gas-liquid, gas-solid, or liquid-solid interfaces. Heat transfer researchers are increasingly interested in developments in noninvasive imaging schemes that allow the reconstruction of three-dimensional interfaces. Problems that are natural candidates for SCM are slowly moving complex interfaces that allow direct optical access but demand high resolution.

6. Acknowledgments

This work was funded under the auspices of the USA National Science Foundation by the Science & Technology Center of Advanced Materials for the Purification of Water with Systems (CAMPWS, cooperative agreement CTS-0120978) and by the Air Conditioning and Refrigeration Center (ACRC) at the University of Illinois at Urbana-Champaign.

7. References

Dyer, J.M., B.D. Storey, J.L. Hoke, A.M. Jacobi, J.G. Georgiadis, (2000) An Experimental Investigation of the Effect of Hydrophobicity on the Rate of Frost Growth in Laminar Channel Flows, *ASHRAE Transactions* **106**(1):143-151.

Georgiadis, J.G., (1994) Multiphase Flow Quantitative Visualization, *Applied Mechanics Review* **47**(6) part 2: S315-S319.

Georgiadis, J.G., (1997) Near-Micron Study of Frost Inception on Substrates Exposed to Humid Air Flow, Oji International Seminar: *New Approach Toward Low-Temperature Thermal Engineering Without Fluorocarbon Refrigerants*, Tomakomai city, Hokkaido, Japan.

Georgiadis, J.G., P. Greywall, and A. Tenbusch, (1994) “Visualization of Hoar Frost with Confocal Microscopy”, in *Transport Phenomena in Solidification,* C. Beckermann et al. (eds.) , ASME **HTD-Vol. 284**: 171-175.

Georgiadis, J.G., M. Ramaswamy, (1995) Thermophysical Manifestations of Frost Inception, Proc. *Symposium on Thermal Science & Engineering in Honor of Chancellor Chang-Lin Tien*, pp. 439-444.

Greywall, P., (1994) *Confocal Microscopy and Magnetic Resonance Imaging of Freezing Interfaces*," M.S. Thesis, University of Illinois at Urbana-Champaign.

Henry, R.C., R.J. Hansmanand, K.S. Breuer, (1995) Heat Transfer Variation on Protuberances and Surface Roughness Elements, *AIAA J. Thermophysics & Heat Transfer*, 9(1): 175-180.

Hoke, J.L. , J. G. Georgiadis, and A. Jacobi, (2004) "The Effect of Substrate Wettability on Frost Properties", *(AIAA) Journal of Thermophysics & Heat Transfer* **18**(2): 228-235.

Hoke, J.L., M. Ramaswamy and J.G. Georgiadis, (2004) "Microscopic Study of Competition between Condensation-Freezing and Ablimation in Supercooled Air Flow", *J. Heat Transfer*, under review.

Kondepudi, S. N., D. L. O'Neal, (1989) Effect of Frost Growth on the Performance of Louvered Finned Heat Exchangers, *Int. J. Refrigeration* **12:** 151-158.

Kondepudi, S. N., D. L. O'Neal, (1990) The Effects of Different Fin Configurations on the Performance of Finned-Tube Heat Exchangers Under Frosting Conditions, *ASHRAE Transactions* **96**(2): 439-444.

O'Neal, D., D. Tree, (1985) A Review of Frost Formation in Simple Geometries, *ASHRAE Transactions* **91**(2): 267-281.

Ramaswamy, M., J.G. Georgiadis, and A. Tenbusch, (1995) Microscopic Study of Frost Inception: Effects of Surface Morphology, Supercooling, and Grazing Flow, ASME preprint **95-WA/HT-22**, International Mechanical Eng. Congress & Exposition.

Sahin, A.Z., (2000) Effective thermal conductivity of frost during the crystal growth period, *Int. J. Heat Mass Transfer* **43:** 539-553.

Seki, N., S. Fukusako, K. Matsuo, S. Uemura, (1984) Incipient Phenomena of Frost Formation, *Bull. JSME* **27**(233): 26-30.

Storey, B.D., A. M. Jacobi, (1999) The effect of stremwise vortices on the frost growth rate in developing laminar channel flows, *Int. J. Heat Mass Transfer* **42:** 3787-3802.

Tao, Y.-X., R.W. Besant, K.S. Rezkallah, (1993) A Mathematical Model for Predicting the Densification and Growth of Frost on a Flat Plate, *Int. J. Heat Mass Transfer* **36**(2): 353-363.

Verwiebe, C., and Ruscheweyh, H., (1998) Recent research results concerning the exciting mechanisms or rain-wind-induced vibrations, *J. Wind Eng. Ind. Aerodynamics*, 74-76, 1005-1013.